Probabilistic Seismic Source Inversion from Regional Landslide Evidence

Ryan A. Rasanen¹ and Brett W. Maurer²

Abstract: In regions of infrequent but potentially damaging seismicity, modern earthquake inventories may be insufficient to provide inputs to seismic-hazard analyses (i.e., fault locations and magnitude-frequency relations). As a result, analysis of paleoseismic evidence, such as coseismic landsliding, is commonly used to help elucidate the seismic record, thereby reducing seismic-hazard uncertainty. However, while paleolandslides have been investigated widely, existing inverse-analysis techniques (i.e., to constrain the causative earthquake magnitude and/or ground motions) have several shortcomings. Namely, they: (i) require the location of the causative earthquake to be known; (ii) provide only a lower-bound estimate of seismic parameters; and (iii) are deterministic in nature. Accordingly, this paper proposes a flexible inversion framework that probabilistically constrains seismic-source parameters from regional paleolandslide evidence. The outputs of this framework are: (i) a geospatial likelihood surface that constrains the location of fault rupture; and (ii) a probability distribution of the rupture magnitude. Simulated paleolandslide studies are performed on modern earthquakes with known parameters. These examples demonstrate the framework's provocative potential as well as important lessons for implementation. The proposed framework has the potential to extract new insights from relic landslide evidence in seismic zones worldwide.

1. Introduction

In many seismic zones, the return period of potentially damaging earthquakes is longer than the duration of seismic observation. As a result, earthquake catalogs may be insufficient to inform the inputs requisite for seismichazard analyses (i.e., the locations, magnitudes, and frequencies of fault ruptures). The uncertainties of these parameters are of significant interest, given that they influence the computed seismic hazard adopted by building codes and used by policy makers (e.g., Vidale et al., 2011). In such cases, paleoseismic relics (i.e., artifacts from pre-historic or pre-instrumental earthquakes) are commonly studied to elucidate the seismic hazard. This includes turbidites (e.g., Goldfinger et al. 2012), tsunami deposits (e.g., Peters et al. 2007), dendrochronology (e.g., Atwater et al. 1991), soil liquefaction (e.g., Maurer et al. 2015), microfossils (e.g., Engelhart et al. 2013), geochemical markers (e.g., O'Donnell et al. 2017), and seafloor morphology (e.g., Watt et al. 2017). Among the many types of such evidence that have been analyzed, paleolandslides are particularly valuable for their ability to "record" the intensity of prior ground motions. This distinction is owed to the fact models exist for predicting landslides as a function of ground motions (or at a minimum, ground-motion intensity measures, IMs). In forward hazard analyses, wherein the seismic loading is given, these models are widely used to predict future landslides. In paleoseismic studies, wherein the outcome is given (e.g., landslides were or were not observed), the models can be inverted to constrain the ground motions that likely would, and would not, produce the observation (e.g., Yagoda-Biran et al. 2010; Wang 2020). Although the date of an earthquake, and thus the recurrence rate, can be derived from many types of evidence, few have a quantifiable relationship with ground motion parameters (e.g., Rasanen et al. 2021). In this respect, paleolandslides are more than just a proxy of past shaking, given that they may quantitatively constrain the motions experienced.

While paleoseismic studies have significant influence on computed seismic hazards in some regions (e.g., Petersen et al. 2008; 2014), paleolandslide research has to-date generally focused more on field investigations (i.e., identification, interpretation, and dating of landslides) and less on advancing the inversion procedures to constrain the causative seismic parameters. All phases of investigation are important, but the focus of this study is on the latter. Notably, existing paleolandslide analysis methods suffer from up to three shortcomings. *First*, existing methods are underpinned by the need to locate the earthquake that induced the observed field of evidence (e.g., earthquake magnitude cannot otherwise be constrained). This requires assumptions in many settings (e.g., where faults are blind or historically quiescent), and in turn, may lead to erroneous characterizations of the seismic hazard. *Second*, existing methods have traditionally analyzed slopes *with* observed landslides (i.e., positive observations) but not slopes *without*

¹ Graduate Research Assistant, University of Washington, Seattle; rrasanen@uw.edu

² Assistant Professor, University of Washington, Seattle; bwmaurer@uw.edu

observed landslides (i.e., negative observations). As a result, derivative estimates of shaking intensity and/or earthquake magnitude are inherently lower-bound estimates, even if this is not explicitly stated. *Third*, existing methods have been deterministic in nature, whereas paleolandslides involve multiple uncertainties that should be accounted for probabilistically to arrive at a transparent and useful characterization of the seismic hazard.

Accordingly, the objective of this paper is to formulate and test a probabilistic framework for inverting seismic-source parameters from ancient landslides. Analyzing regional evidence, this framework computes the likelihood of a rupture with given location, geometry, and magnitude producing a set of field observations, wherein various measurement and modelling uncertainties may be included. Repeating for a near-infinite number of possible faults results in a regional-scale understanding of the likely source parameters. The degree of successful constraint will be investigated using tests on modern earthquakes with known parameters. That is, simulated paleolandslide studies will be performed to assess the framework's efficacy. In the following, existing paleolandslide analytics are briefly summarized, to include discussion of the aforementioned shortcomings. An overview of the framework proposed herein is then given, followed by specific implementation details. Lastly, tests of the framework on four modern earthquakes are presented, from which important lessons and caveats for forward use are gleaned.

1.1 Existing Paleolandslide Analytics and Their Shortcomings

Paleolandslide studies can potentially provide information about the dates, locations, and magnitudes of paleoearthquakes, as well as the resultant, regionally distributed ground motions. A complete study of paleolandslides is three phased: (i) field identification and interpretation; (ii) dating; and (iii) constraint of the earthquake magnitude and/or ground motion under which the field of evidence was formed. Interpreting whether a paleolandslide is of seismic origin is inherently challenging. Crozier (1992), for example, proposed six criteria for this purpose, as based on observations in New Zealand. In general, the most important markers of seismic origin are: (i) multiple spatiotemporally clustered landslides for which (ii) static slope-stability analyses predict stability even in saturated conditions; and where (iii) other paleoseismic evidence of the same age is also found. For overviews of field identification and interpretation, the reader is referred to Jibson (1996) and Clague (2014), which may be complimented with specific case studies that highlight the use of remote-sensing technology (e.g., Sutinen et al. 2014). Once identified, paleolandslides may be dated via radiocarbon (e.g., Stout 1977; Ojala et al. 2018); optically stimulated luminescence (e.g., Katz et al. 2011); dendrochronology (e.g., Hupp et al. 1987; Struble et al. 2020), cosmic ray exposure (e.g., Le Roux et al. 2009; Mackey and Quigley 2014), and several relative dating approaches (e.g., lichenometry – Bull et al. 1994), among others. Ideally, multiple dating methods are used to reduce uncertainty (Johnson 1987). A comprehensive overview of dating methods is given by Jibson (1996) and Panek (2015). Panek (2015) also provides a list of regions with well-established landslide chronologies. These regional chronologies excellent examples of which include Chen et al. (2012) and Martino et al. (2014) – form both the basis of paleoseismic research and the landslide inventories required to train and test improved landslide prediction models. In some cases, these chronologies may provide more recent analog events that aide in the interpretation of older paleoearthquakes.

Following field interpretation, dating, and inventorying, the techniques by which the causative earthquake magnitude and/or shaking intensity are quantitatively constrained are generally called back- or inverse-analysis methods. While several such methods have been used, we refer to the two most common and credible to-date as the "magnitude-bound" method (e.g., Keefer 1984; Rodriguez et al. 1999; Papadopoulos and Plessa 2000; Delgado et al. 2011) and the "site-specific stability analysis," or for brevity, the "site-specific" method (e.g., Jibson and Keefer 1993; Strasser et al. 2006; Yagoda-Biran et al. 2010; Wang 2020; Junquera-Torrado et al. 2021).

The magnitude-bound method uses a correlation relating earthquake magnitude to the site-to-source distance of the most distal landslide observation (typically in terms of epicentral distance). Variants of this method relate earthquake magnitude to the area affected by landslides (e.g., Tanyas et al. 2018). Developed from observations in modern earthquakes, these correlations traditionally use empirical data from variable geologic-tectonic settings. As an example, Fig. 1 presents the magnitude-bound correlation developed by Keefer (1984) using data from 40 global earthquakes that occurred AD 1811-1980. This curve can be used to estimate the lower-bound magnitude required to induce landslides at a given site-to-source distance. Subsequent authors (e.g., Rodriguez et al. 1999; Delgado et al.

2011) have generally corroborated the Keefer (1984) curves for more recent earthquakes. The shape of any such curve is a function of seismic source, path, and site effects (e.g., rupture mechanism, ground motion attenuation, and site effects), as well as landslide susceptibility (e.g., strength parameters, slope angle, and water table location). Because these factors vary spatially, region-specific correlations may provide more accurate estimates than those developed from global data (e.g., Papadopoulos and Plessa 2000; Chen et al. 2012; Martino et al. 2014; Comerci et al. 2015). As evident from Fig. 1, application of this method results in constraint of a paleoearthquake's magnitude, wherein the maximum site-to-source distance of landsliding is the only required input. Knowing or estimating the source location is thus critical, yet the magnitude-bound method provides little means to locate it. Additionally, as a lower-bound method, the actual magnitude is potentially much larger than predicted. But, despite the uncertainties inherent to magnitude-bound curves, probabilistic correlations have yet to be developed. Is it thus unclear what a "lower bound" prediction is in statistical terms.

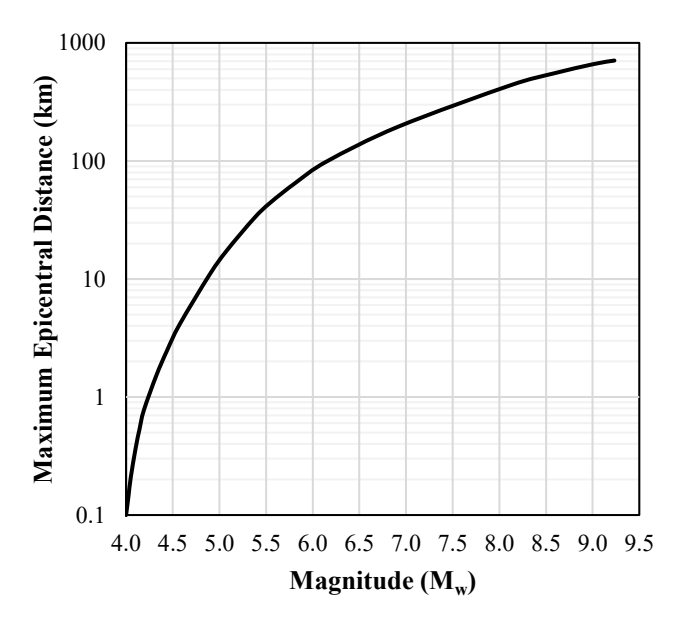


Fig. 1. Magnitude-bound curve proposed by Keefer (1984) for world-wide earthquakes, where site-to-source distance is quantified in terms of maximum epicentral distance to disrupted landslides.

The second, more technical site-specific method uses a dynamic slope-stability analysis based on some combination of geospatial, geologic, and geotechnical measurements. Several approaches of differing sophistication are available to predict dynamic slope stability, depending on the degree to which site-specific profiling and measurements are available. These include empirical (e.g., Nowicki et al. 2018), limit equilibrium (e.g., Morgenstern and Price 1965), sliding block (e.g., Jibson 1993), and non-linear dynamic models (e.g., Boulanger 2019). In a paleoseismic analysis, wherein the outcome is given (i.e., landslides did or did not occur), any of these models can be used to determine ground motions that likely would, and would not, produce the observed outcome. While implementations have varied greatly with time and place (e.g., Jibson and Keefer 1993; Strasser et al. 2006; Yagoda-Biran et al. 2010; Meunier et al. 2013; Wang 2020; Junquera-Torrado et al. 2021), the site-specific method can: (i) constrain ground-motion parameters likely to produce outcomes at individual sites; and (ii) by analyzing regional evidence, give an estimate of the causative earthquake magnitude. If, for example, a slope-stability model was adopted that characterized seismic demand in terms of earthquake magnitude (M_w) and some intensity measure (IM), then a limit-state condition could, for a given slope, be computed to separate combinations of M_w and IM sufficient to induce landsliding from combinations that are insufficient. This is shown conceptually in Fig. 2a. Because there are infinitely many such combinations, a ground-motion model (GMM) is used to determine credible combinations for a given site, as shown in Fig. 2b (dashed line), where the GMM predicts the IM as a function of M_w and site-to-source distance (R), among other factors. As indicated in Fig. 2b, the portion of this line plotting above the defined limit state corresponds to credible M_w -IM combinations that could induce a landslide at the site, given a rupture at some distance R. The intersection of the GMM with the limit state thus defines the minimum M_w expected to induce a landslide.

As evident from Fig. 2, site-to-source distance must be known to perform the site-specific method, as it presently exists. This can lead to inaccurate assumptions, and by corollary, erroneous results (e.g., where fault locations are unknown, or where prospective causative faults are plentiful). In addition, implementations of this method (e.g., Jibson and Keefer 1993; Strasser et al. 2006; Yagoda-Biran et al. 2010; Wang 2020; Junquera-Torrado et al. 2021) have ignored negative observations (i.e., slopes without landslides), the analysis of which would result in an upper-bound M_w -IM combination (i.e., had the seismic loading been larger, a landslide would be expected). Moreover, existing implementations have not considered the uncertainties inherent to ground-motion and landslide prediction. These implementations thus have the same shortcoming as the magnitude-bound method in that they provide a deterministic, lower-bound constraint on the causative earthquake magnitude.

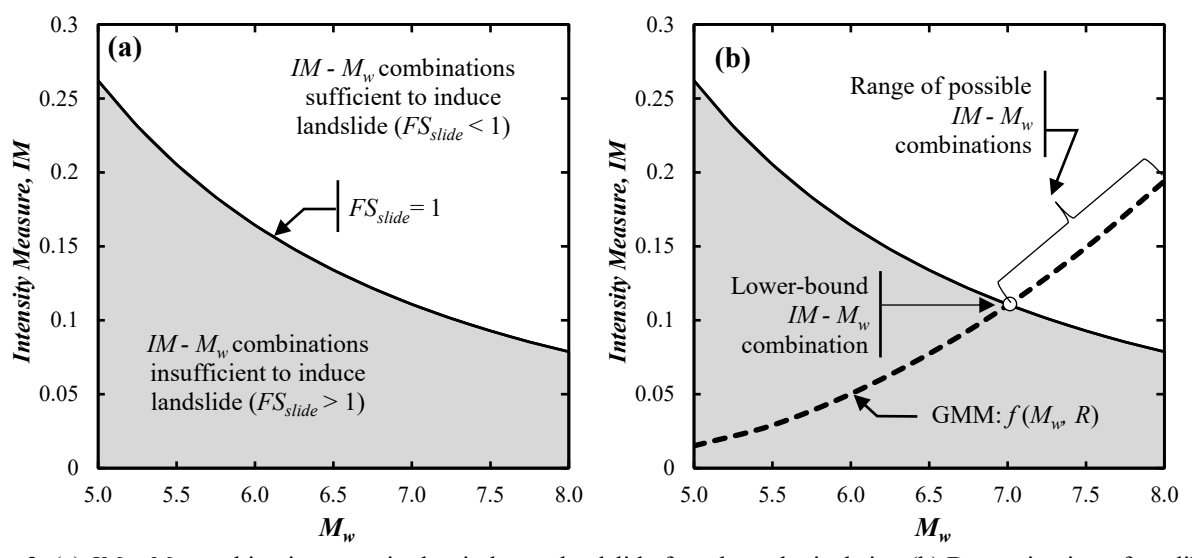


Fig. 2. (a) $IM - M_w$ combinations required to induce a landslide for a hypothetical site; (b) Determination of credible lower-bound $IM - M_w$ combination. GMM = ground motion model.

2. Methodology

The proposed framework is described in two parts. The first presents a conceptual overview and simple hypothetical application. The second provides implementation details to assist analysts in applying the framework, and to describe the validation tests that will be performed subsequently.

2.1 Overview of Proposed Framework

Analyzing regional paleolandslide evidence, the proposed framework aims to probabilistically constrain the causative seismic source from a near-infinite number of possibilities. This will be accomplished by assessing the likelihood that a rupture with given location, geometry, and magnitude would produce a series of field observations (sites with and without landslides) wherein uncertainties inherent to ground motion and landslide modelling may be considered. In general, the likelihood of a parameter having a value, given a set of observations, is the product of the probabilities of those observations, conditioned on the parameter value. The likelihood of a seismic source having some location (L), geometry (G), and magnitude (M_w) , given a set (x) of field observations at N different sites, can thus be computed as:

Likelihood
$$(L, G, M_w | x) = P(X = x | L, G, M_w) = \prod_{i=1}^{N} P(X_i = x_i | L, G, M_w)$$
 (1)

Where $P(X_i = x_i | L, G, M_w)$ is the probability of the observation at site *i* (landslide or no landslide) given an earthquake with parameters L, G, and M_w . By repeating for a near-infinite number of possibilities, the most likely, actual rupture parameters are probabilistically constrained via the likelihood function (product of the probabilities of N observations), such that different combinations of L, G, and M_w will be found more and less likely to produce the observed field evidence. In Eq. (1), the probability of a field observation, conditioned on all input variables, is computed at sites with and without landslides using Eqs. 2a and 2b, respectively:

$$P(\text{Landslide}|\text{EQK}: L, G, M_w) = \int_{IM} P(\text{Landslide}|IM) f(IM|L, G, M_w) \cdot dIM$$
 (2a)

$$P(\text{No Landslide}|\text{EQK}: L, G, M_w) = 1 - \int_{IM} P(\text{Landslide}|IM) f(IM|L, G, M_w) \cdot dIM$$
 (2b)

Where $f(IM|L, G, M_w)$ is a probability density function (PDF) computed by a ground motion model (GMM) considering site response, and conditioned on fault parameters L, G and M_w ; and P(Landslide|IM) is the probability of observing a landslide, given ground-motion intensity measure IM, as computed by a landslide prediction model.

The proposed framework is demonstrated conceptually in Fig. 3 considering four hypothetical field sites, where a landslide is observed at site numbers one and two, but not at site numbers three and four, and two possible source locations for the earthquake that produced the observations. In actual analyses, a near-infinite number of source locations may be considered. Fig. 4 illustrates how the relative likelihoods of locations one and two are assessed. Shown in Fig. 4a are the probabilities of individual field observations, given an earthquake at location one, as computed by Eq. 2 for varying M_w . At sites with a landslide, the probability of the field observation increases with increasing M_w , whereas at sites without a landslide, the opposite occurs. In Fig. 4b, this process is repeated considering an earthquake at source location two. In Fig. 4c, the likelihood of each source location is computed as a function of $M_{\rm w}$, per Eq. 1 (the product of the black and gray curves). It can be seen that location one has a far greater peak likelihood, whereas an earthquake at location two is unlikely to produce the field observations, regardless of its M_{W} . Repeating this process at a near-infinite number of locations, a geospatial surface of peak likelihood can be developed, potentially constraining the location of fault-rupture. Moreover, for any location considered, the likelihood distribution of earthquake magnitude is computed, as shown in Fig. 4c. This can be interpreted as a PDF of the causative earthquake magnitude, conditioned on a seismic-source location. By aggregating PDFs from potential source locations across the study area, an overall PDF of earthquake magnitude, considering all possible source locations, is produced. In situations where the source location is well constrained, the overall PDF is similar to the PDF conditioned on a single, most likely source location. In contrast, when the source location is less well constrained (e.g., due to limited field evidence), the overall PDF is wider than that conditioned on the single most-likely location. Collectively, these products (i.e., probability distributions of rupture location and magnitude) are inputs to regional and national probabilistic seismic hazard analyses.

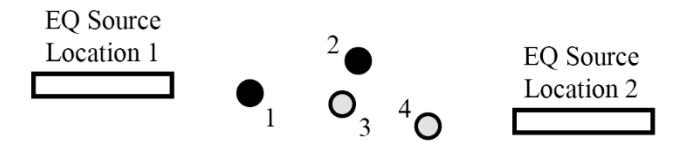


Fig. 3. Hypothetical paleolandslide analysis consisting of four field sites, where a landslide was observed at sites one and two (black circles), but not at sites three and four (gray circles). Also shown are two possible sources for the earthquake that produced these observations.

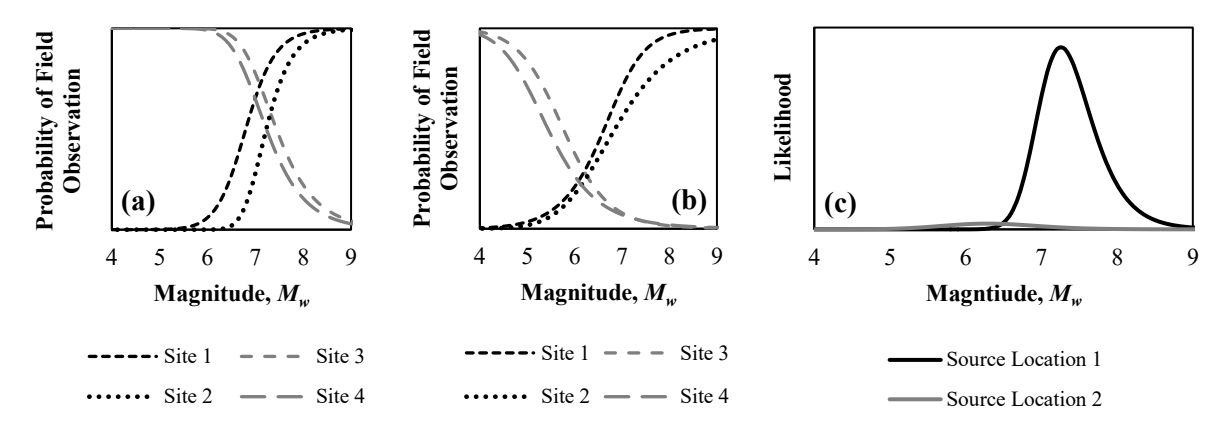


Fig. 4. Conceptual illustration of the proposed framework for locating the source of the earthquake that produced the field observations depicted in Fig. 3: (a) probabilities of field observations, given an earthquake at location one of varying M_w ; (b) probabilities of field observations, given an earthquake at location two of varying M_w ; (c) likelihood vs. M_w for source locations one and two.

2.2 Implementation Details

The implementation of Eqs. 1 and 2 is next discussed in detail. This includes general concepts, as well as the specific methods and models adopted herein for application to four modern earthquakes. While further details will be provided later, the framework will be applied to four events in California, USA, from which landslide inventories are available in Schmitt et al. (2017): (i) 1971 Mw6.6 San Fernando; (ii) 1983 Mw6.7 Coalinga; (iii) 1989 Mw6.9 Loma Prieta; and (iv) 1994 Mw6.7 Northridge. Owing to the modular form of the proposed framework, in which ground motions and landslides are separately predicted in series, it is easily modified for alternative and future prediction methods. In this regard, the Nowicki et al. (2018) landslide model, which uses geospatial variables, will be adopted in the current study for its ease of application. Using this model, the probability of a landslide, P(x), is:

$$P(x) = \frac{1}{1 + e^{-x}}$$
 (3) where $x = a + b \times \ln PGV + c \times Slope + d \times Lithology + e \times Land Cover + f \times CTI + g \times \ln PGV \times Slope$

In Eq. (3), coefficients a through f are logistic regression coefficients trained on 23 landslide inventories. PGV is peak ground velocity (cm/sec); Slope is the ground slope (degrees) computed from the 7.5 arc-second resolution Global Multi-resolution Terrain Elevation Data (GMTED) (Danielson and Gesch, 2011); Lithology is obtained from the global lithology (GLiM) database of Hartmann and Moosdorf (2012); $Land\ Cover$ is obtained from the global land cover (GlobCover) maps of Arino et al. (2012); and CTI is the compound topographic index (a proxy for soil wetness) and is obtained from the Hydrologic Derivatives for Modeling and Analysis (HDMA) database (Verdin 2017). Per the recommendation of the U.S. Geological Survey (USGS 2021) who use the Nowicki et al. (2018) model in post-earthquake data products, we: (i) exclude areas with slopes less than 5°; and (ii) revise the lithologic 'd' coefficient for "unconsolidated sediments" from -3.22 to -1.36, which is the coefficient for "mixed sedimentary rocks" to better reflect that this unit is expected to be weak. Mapped in Fig. 5 for the Los Angeles metropolitan region, which will be studied herein, are the four "capacity" variables used by the Nowicki et al. (2018) model.

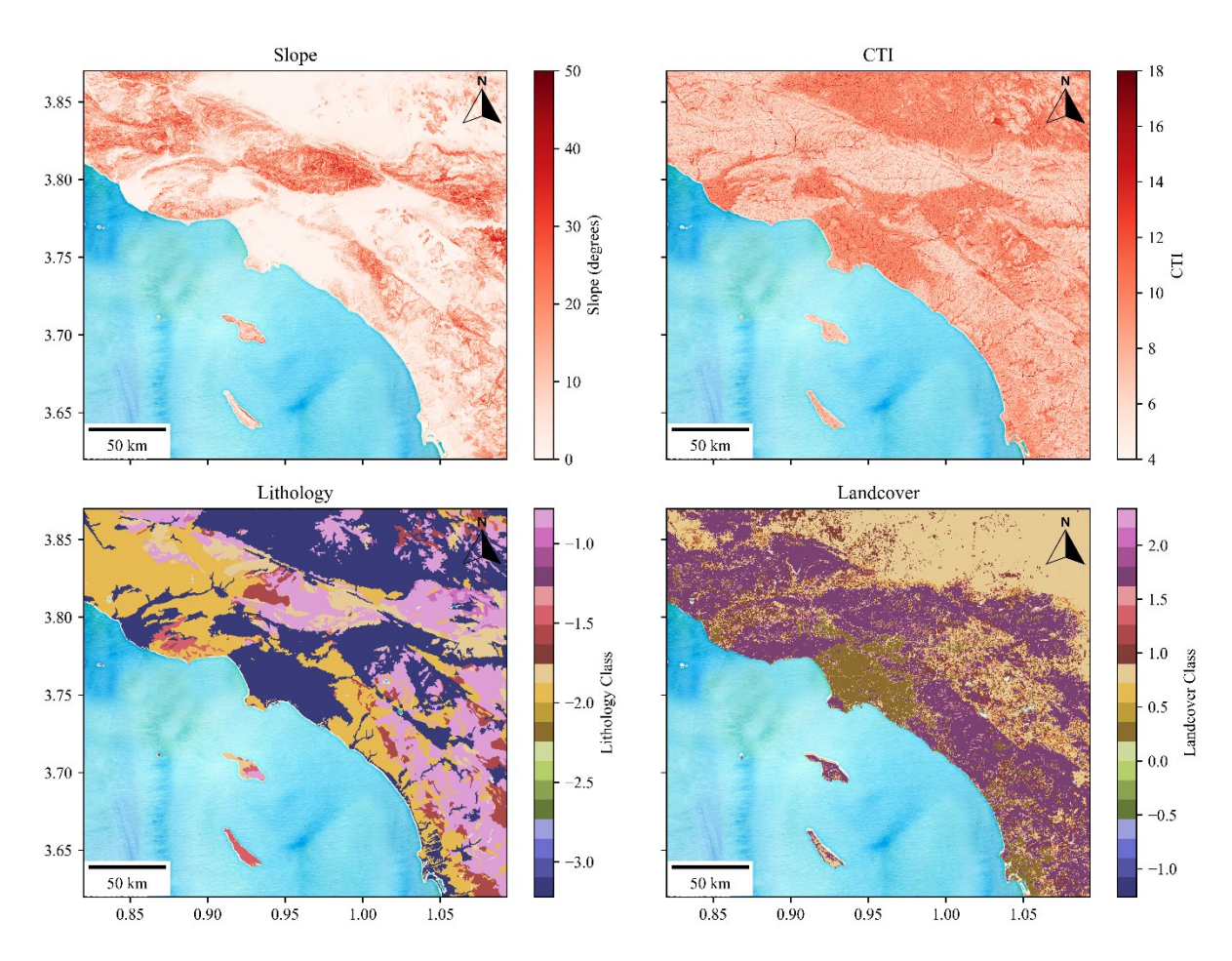


Fig. 5. Geospatial capacity variables used by the Nowicki et al. (2018) landslide model.

While empirical hazard models like Nowicki et al. (2018) have outperformed mechanistic models in some settings (Geyin et al. 2020), we generally assume that the adopted model is not the most accurate available. However, this model allows for the proposed framework to be readily implemented on multiple events, each with numerous study sites. In a paleolandslide study, wherein site- or region-specific profiling and material shear-strengths may be available, an improved empirical or mechanistic landslide model could be employed (e.g., limit equilibrium, sliding block, or nonlinear dynamic analysis). In cases where the mode of landsliding may be discerned, mode-dependent models, which potentially offer improved prediction efficiency, could be used. The basic approach, however, would not otherwise be different. To implement the framework, an analyst must:

- (1) Create an array of possible source locations. In this paper, a 250 km by 250 km grid of surficial points, which will be treated as possible earthquake epicenters, was adopted and centered on the landslide field, such that the grid's borders far exceed the extent of landslides. Within the grid area (62,500 km² in this study), a finer point spacing gives greater spatial resolution while a coarser spacing allows for faster runtime. Balancing these ideals, a 1 km spacing was adopted for a 10,000 km² area at the center of the grid, while a 10 km spacing was adopted for the remainder of the 62,500 km² study area. In the event that points in the coarsely-spaced region are identified as likely sources, the grid can be recast at higher spatial resolution (i.e., to further constrain the likely source location, if possible).
- (2) Select *N* study sites where the presence or absence of landslides was observed. Ideally, and as implemented in this work, an equal number of sites with and without landslides is selected to limit sampling bias.

- (3) Select an appropriate GMM for the parameters required by the landslide model. In this paper, the Chiou and Youngs (2014) GMM for crustal earthquakes in active tectonic settings was adopted to predict *PGV* in all events.
- (4) For each provisional seismic-source locale created in (1):
- (5) For each provisional seismic-source M_w being considered (a range of M_w 5 to M_w 9 was used in this paper, in increments of $0.1M_w$, with the M_w 5 lower limit chosen following Keefer (1984)):
- (6) For each of N study sites selected in (2), cycling from i = 1 to N:
- (7) Compute the site-to-source distance(s) required by the GMM chosen in (3), as measured from study site i to the provisional seismic sources. In this paper, the required metrics include Joyner-Boore distance (R_{JB}) and the closest distance to fault rupture (R_{RUP}). Since the seismic sources generated in (1) are epicenters, rather than 3-dimensional faults, the correlations of Scherbaum et al. (2004) were used to estimate R_{JB} from epicentral distance (R_{EPI}), assuming a strike-slip fault with dip (δ) of 90°. The Scherbaum et al. (2004) correlations, which are magnitude dependent, effectively convert the point sources from (1) into a statistical realization of a 3-dimensional fault. R_{RUP} was calculated per the Pythagorean theorem using estimates of R_{JB} (computed as in the above) and the depth to top-of-rupture (Z_{TOR}). Z_{TOR} was estimated using the correlation of Kaklamanos et al. (2011), which requires as inputs the: down-dip rupture width (W); hypocentral depth (Z_{HYP}); and δ . Following the recommendation of Kaklamanos et al. (2011), W and W were respectively estimated per the methods of Wells and Coppersmith (1994) and Scherbaum et al. (2004). It should be noted that the Scherbaum et al. (2004) R_{JB} correlation was used beyond the 5.0 < M_W < 7.5 parameter space of the data used to train it. As a result, some adjustments to physically indefensible values were needed at very small and large M_W : (i) if $R_{JB} > R_{EPI}$, $R_{JB} = R_{EPI}$; (ii) if $R_{JB} < 0$, $R_{JB} = 0$.
- (8) Using the GMM selected in (3) and site-to-source distances from (7), compute the PDF of expected PGV at study site i, wherein the time-averaged shear wave velocity over the top 30 m (V_{S30}) is consistent with site i. In this paper, the fault source was assumed to have strike-slip parameters ($\delta = 90^{\circ}$ and rake, $\lambda = 0^{\circ}$) and V_{S30} was estimated by the method of Heath et al. (2020). Topographic amplification was not considered but could be if incorporated into future GMMs. In general, the probability distribution of PGV is assumed to be a lognormal random variable defined by the median and lognormal standard deviation provided by the GMM. In this paper, PGV predictions beyond +/- 3 standard deviations of the median are truncated, as is typical in ground-motion modeling (since such values may be physically impossible) and the PDF is scaled upwards such that the area under the truncated PDF is one.
- (9) For each possible PGV value at study site i, as computed in (8) for a given M_w and site-to-source distance pair (a PGV increment of 5 cm/s was adopted in this paper):
- (10) Compute the probability of a field observation using Eq. 2a or 2b, depending on whether landslides were or were not observed at study site *i*. Completing these equations (i.e., by summing over all PGV values) gives the probability of field observation at site *i* for a given provisional source location and M_w . Repeating steps 6-10 for each provisional M_w being considered results in a probability of field observation versus M_w curve for each study site, examples of which are shown in Figs. 4a and 4b.
- (11) Compute the likelihood of a provisional source locale, as a function of M_w , by multiplying the probabilities of field observations at all study sites (i.e., multiply the curves shown in Fig. 4a or 4b at each value of M_w). The result, an example of which is shown in Fig. 4c, is akin to a PDF of the causative earthquake magnitude, conditioned on a single seismic-source location.
- (12) Repeating steps 5-11 for all provisional seismic source locations created in (1) results in a likelihood distribution for each, as described in (11).
- (13) Following from (12), normalize the peak likelihood at each source location by the peak likelihood among all locations. This allows for the relative likelihoods of source locations to be assessed, with the most likely location having a normalized value of one. The M_w corresponding to the peak likelihood (see Fig. 4c) is the median M_w likely to produce the field observations, given that an earthquake at the source location occurs.
- (14) From the arrays of normalized likelihood and median M_w , create geospatial surfaces or contours to identify the most-likely source location and median M_w , conditioned on that location.
- (15) Finally, by aggregating PDFs from all potential source locations across the study area, an overall PDF of earthquake magnitude, considering all possible source locations, is produced. While a single source location will always be deemed "most likely," earthquakes at multiple other source locations have potential to produce the field of evidence,

albeit with lesser likelihood. In general, this overall PDF will be wider (i.e., have greater uncertainty) than the PDF conditioned on the single most likely source, especially when the source zone is not well constrained (e.g., due to limited field evidence).

3. Simulated Application

The proposed framework, as outlined above, provides probabilistic constraint on both the location and M_w of a seismic event considering landslide evidence. To investigate the degree of successful constraint and glean lessons for future use, simulated paleolandslide studies are next performed on four modern events with known seismic sources. As in any paleolandslide analysis (and paleoseismic research in general), the need exists, where judicious, to classify sites as "positive" and "negative" (i.e., landslides are, or are not, present). Inherent to the subsequent applications, it is thus assumed that the presence or absence of landslides would be accurately interpreted in a paleoseismic investigation, and moreover, that landslides would be properly attributed to a causative earthquake. These assumptions are not intended to diminish the importance of interpreting and dating earthquake-induced landslides in the field, which is both difficult and uncertain. The objective herein is to advance seismic-source inversion techniques, rather than to discuss or simulate the field investigations prerequisite for all such analyses.

In each event, the inverted, probabilistic source location and magnitude will be compared to the actual, known parameters. However, no prior knowledge of the seismic source is incorporated into the analyses. In addition, because the four earthquakes are modern, the number of study sites available from reconnaissance (i.e., slopes with and without observed landslides) is very large (e.g., 10,000+ in some events). Given that this far exceeds the number of field sites conceivable of a regional paleolandslide study, analyses will be performed on randomly selected samples of 100 study sites from each event (50 slopes with observed landslides, 50 slopes without). Because modern landslide inventories are comprised almost exclusively of positive observations, we assume slopes within a given survey area did not experience slides if none are mapped. While this inevitably introduces uncertainty, it facilitates rapid implementation of the proposed framework and is not dissimilar from a paleoseismic study, wherein an absence of evidence may not be evidence of absence. The preservation and sampling of evidence is further discussed later in the paper.

3.1 San Fernando, California

The 1971 M_w 6.6 San Fernando, California earthquake occurred on the Sierra Madre Fault (Carena and Suppe 2002). An inventory of observed landslides was obtained from Morton (1971), as compiled by Schmitt et al. (2017), and is mapped in Fig. 6a. A representative example of the framework's output is in Fig. 6 for an analysis using 100 randomly selected study sites; the surface projection of the 1971 fault rupture is also shown. Mapped in Fig. 6a are contours of relative likelihood, wherein values near one and zero respectively denote source locations most and least likely to produce the observed evidence. Mapped in Fig. 6b are contours of M_w , indicating the rupture magnitude most likely to produce the observed evidence, given an earthquake at that location (i.e., the median M_w , conditioned on location).

As seen in Fig. 6a, the analysis identified a relatively well-constrained area as the likely source. This aligns with the actual rupture, such that the identified, most likely source falls within the surface projection of the fault that ruptured. In addition to this fault, other known faults in the region are mapped, such that their computed potential to produce the evidence field may be assessed. It can be seen that other potential seismic sources in the region are all judged unlikely to produce the observed evidence. As shown in Fig. 6b, the median magnitude corresponding to the most-likely source location was $M_w 6.6$, matching the actual magnitude. Because M_w contours tend to map as concentric circles centered on the evidence field, as in Fig. 6b, these contours are provided in Appendix A for the remainder of events. In addition to the median M_w of $M_w 6.6$, other M_w values at the most-likely source location could inevitably produce the evidence field (e.g., if ground motions were higher or lower than the median expectation). Shown in Fig. 7a is the full PDF of M_w , conditioned on the most likely source location, which is analogous to the conceptual PDFs shown in Fig. 4c. The 95% confidence interval (CI) is $M_w 6.25$ - $M_w 6.80$. Moreover, as shown in Fig. 6a, earthquakes elsewhere have potential to produce the evidence field, albeit with lesser likelihood. By aggregating individual PDFs from all locations across the 62,500 km² study grid, an overall PDF that includes source-location uncertainty is produced. This PDF, which is also shown in Fig. 7a, has a median of $M_w 6.6$ and 95% CI of $M_w 6.25$ -

 M_w 6.90. Unless the causative fault can be constrained via on-fault (or some other) evidence, this latter, more uncertain PDF would be the more appropriate product of a paleolandslide analysis.

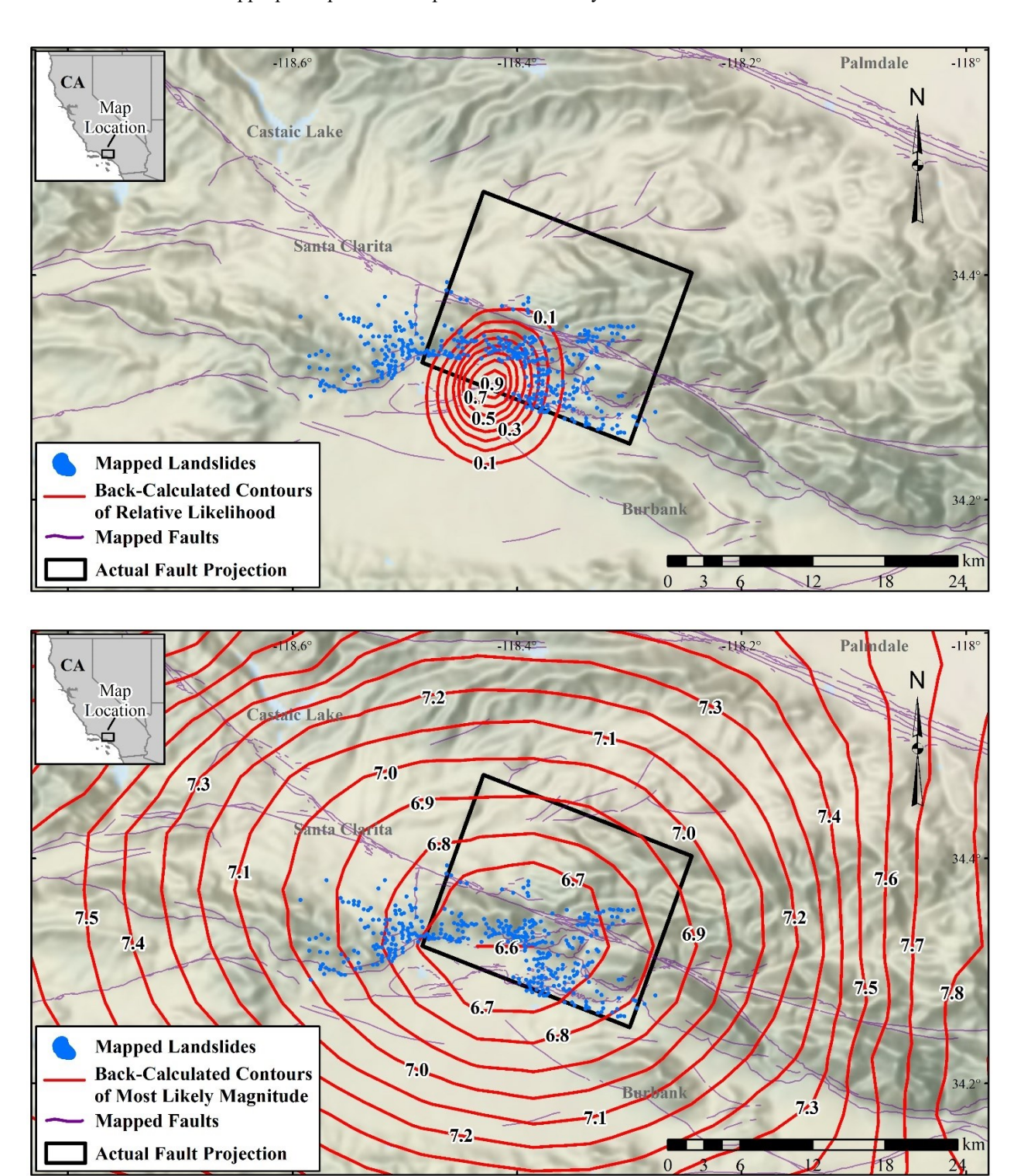


Fig. 6. Representative analysis of 100 study sites (50% positive, 50% negative) randomly selected from the 1971 M_w 6.6 San Fernando, California earthquake inventory: (a) contours showing the relative likelihood of earthquake source locations; and (b) corresponding M_w most likely to produce the field evidence, if the earthquake occurred at a

given location. Black rectangles = actual fault projection (Carena and Suppe 2002); faint purple lines = other mapped faults in the region (California Geological Survey 2014); blue polygons = complete inventory of mapped landslides.

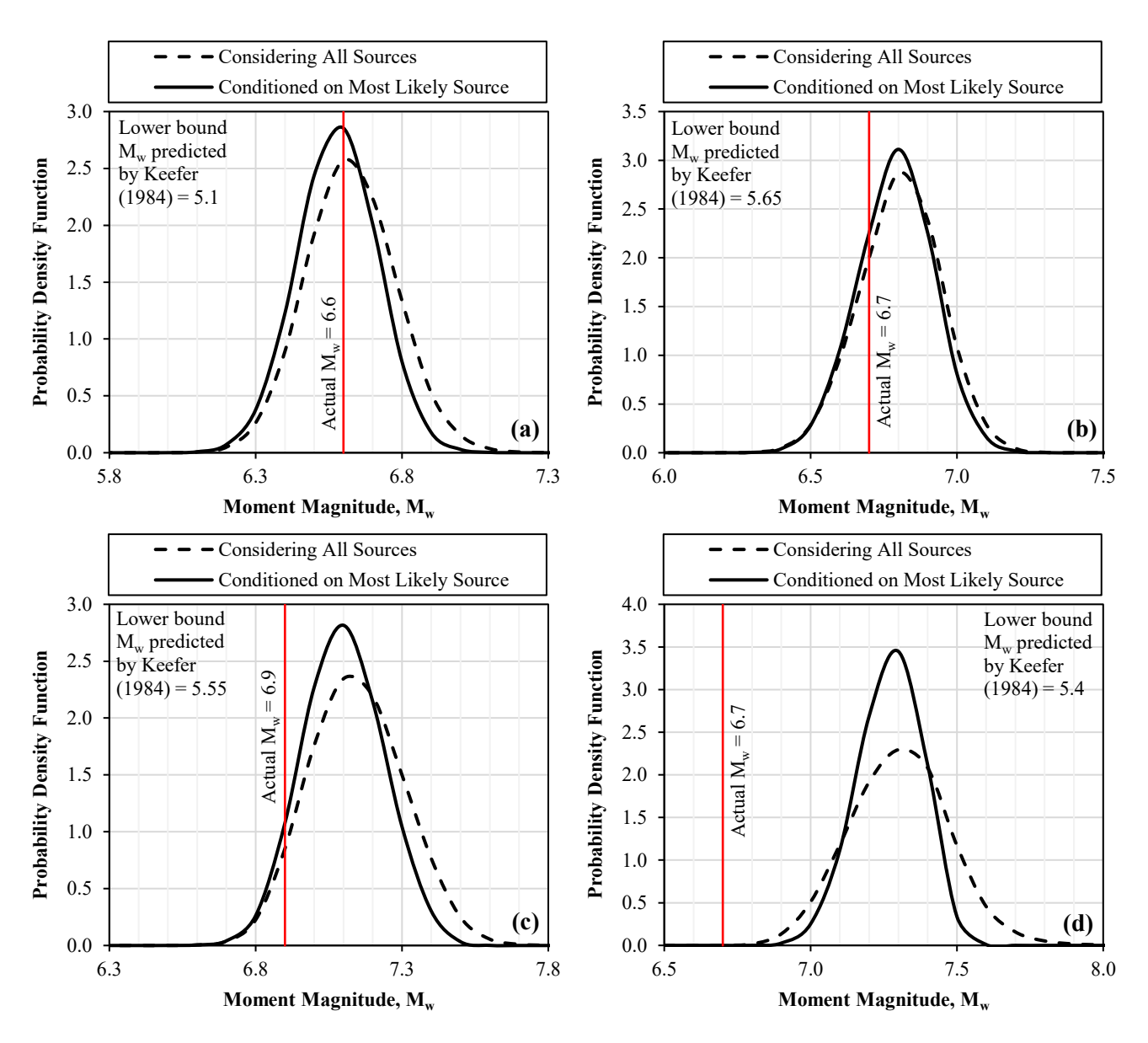


Fig. 7. PDFs of earthquake magnitude inverted from regional landslide evidence in the: (a) 1971 M_w 6.6 San Fernando; (b) 1994 M_w 6.7 Northridge; (c) 1989 M_w 6.9 Loma Prieta; and (d) 1983 M_w 6.7 Coalinga earthquakes. Shown are the PDFs conditioned on the most-likely source location (solid lines) as well as the aggregate PDFs considering source-location uncertainty (dashed lines).

For comparison, the magnitude-bound curve of Keefer (1984) (later corroborated by others) was used to predict the magnitude of the event, as has been employed in paleoseismic studies. To do so, the centroid of all mapped landslides was assumed to be the source location, from which the site-to-source distance of the most distal landslide was measured to obtain a minimum magnitude of M_w 5.1 using Fig. 1. Applications of the "site-specific" approach, wherein a minimum ground-motion for sliding is established, would similarly result in a lower-bound magnitude. By contrast, the proposed framework allows for all uncertainties to be considered, resulting in a more meaningful,

probabilistic understanding of source location and magnitude. In general, as the number of field sites increases, the uncertainty bounds on location and magnitude decrease, and vice-a-versa.

3.2 Northridge

The 1994 M_w 6.7 Northridge, California earthquake occurred on a deeply buried blind thrust fault (Updike et al. 1996) in proximity to the 1971 San Fernando event. Landslide inventories were obtained from Harp and Jibson (1995) and Townsend et al. (2020), as compiled by Schmitt et al. (2017), and are mapped in Fig. 8. A representative output is shown in Fig. 8 for an analysis using 100 random study sites; the surface projection of the 1994 fault rupture is also shown. Mapped in Fig. 8 are contours denoting source locations most and least likely to produce the observed evidence. The analysis again identified a relatively well-constrained area as the likely source, ~12 km NW of that predicted for the 1971 San Fernando event. It can also be seen that the source with greatest likelihood is ~5 km from the actual fault projection, but that locations within the projection do have up to 40% relative likelihood (i.e., they are not unlikely). The median M_w (See Appendix A) at the most-likely source was M_w 6.8 with a 95% CI of M_w 6.5- M_w 7.0, versus the actual M_w 6.7. As with the San Fernando earthquake, this PDF - conditioned on the most-likely source location - and the overall PDF reflecting source-location uncertainty, are computed and shown in Fig. 7b. In this analysis, the two PDFs provide essentially the same M_w distribution. For comparison, the Keefer (1984) magnitude-bound curve was used to predict the magnitude as previously described. This resulted in a lower-bound estimate of M_w 5.65. Thus, the proposed framework provides results that are informative, even if imperfect, especially when considering that an empirical landslide model using few site-specific parameters is being employed.

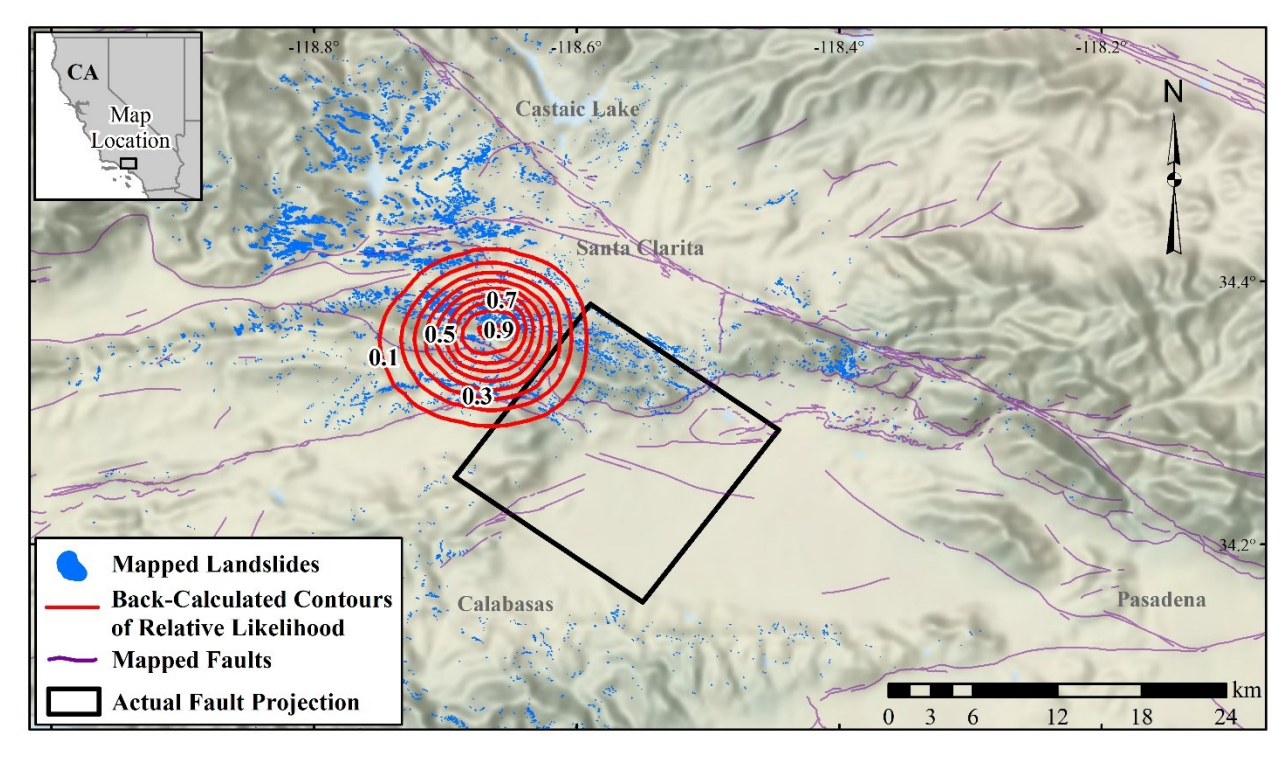


Fig. 8. Representative analysis of 100 study sites (50% positive, 50% negative) randomly selected from the 1994 M_w6.7 Northridge, California earthquake inventory: contours showing the relative likelihood of earthquake source locations. Black rectangles = actual fault projection (Updike et al. 1996); faint purple lines = other mapped faults in the region (California Geological Survey 2014); blue polygons = complete inventory of mapped landslides.

3.3 Loma Prieta

The 1989 $M_w6.9$ Loma Prieta earthquake occurred on the San Andreas Fault (Wald et al. 1991). An inventory of observed landslides was obtained from Keefer and Manson (1998), as compiled by Schmitt et al. (2017), and is mapped in Fig. 9. The results of a representative analysis of 100 study sites are also shown. The inversion identified a most-likely source approximately ~2 km from the actual fault projection, with some locations in the projection having up to 90% relative likelihood. The corresponding median magnitude was $M_w7.1$ (Appendix A), with a 95% CI of $M_w6.8$ - $M_w7.3$, as shown in Fig. 7c. Aggregating conditional PDFs from across the study area resulted in an overall PDF with median $M_w7.1$ and 95% CI of $M_w6.8$ - $M_w7.4$, versus the actual $M_w6.9$. By contrast, the Keefer (1984) magnitude-bound curve gives a lower-bound estimate of M_w 5.5. Thus, similar to the 1994 Northridge earthquake, the actual source parameters (i.e., location and magnitude) fall within the inverted distributions, even if not precisely at the medians.

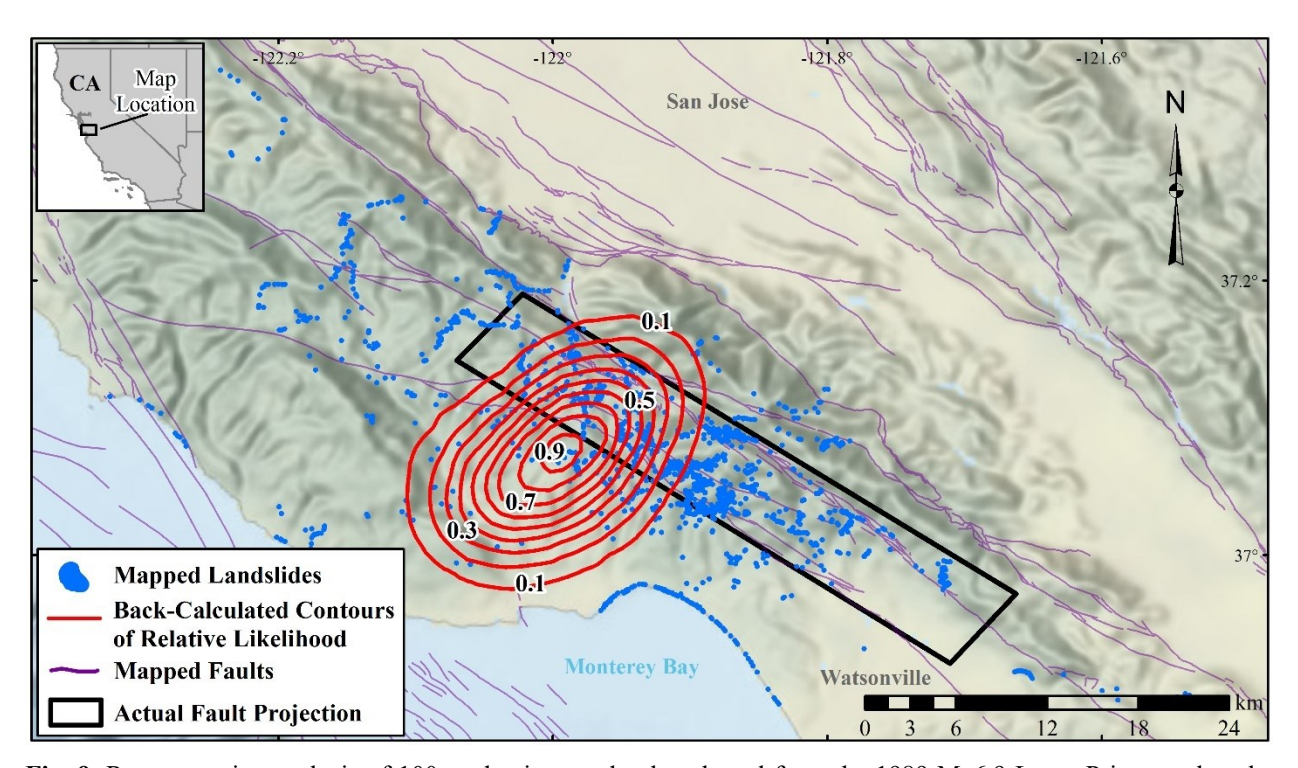


Fig. 9. Representative analysis of 100 study sites randomly selected from the 1989 M_w 6.9 Loma Prieta earthquake inventory: contours showing the relative likelihood of source locations. Black rectangles = actual fault projection (Wald et al. 1991); faint purple lines = other mapped faults in the region (California Geological Survey 2014); blue polygons = complete inventory of mapped landslides.

3.4 Coalinga, California

The 1983 M_w 6.7 Coalinga earthquake occurred on a previously unknown fault along the structural boundary of the San Joaquin Valley (Wentworth and Zoback 1990). An inventory of observed landslides was obtained from Harp and Keefer (1990), as compiled by Schmitt et al. (2017). The result of a representative analysis of 100 study sites is shown in Fig. 10. The inversion accurately located the source, with the identified, most-likely grid point falling within the actual fault projection. However, the median inverted M_w here (See Appendix A) was M_w 7.3 with 95% CI of M_w 7.0- M_w 7.4, as shown in Fig. 7d. In contrast, the actual magnitude, M_w 6.7, was deemed to have near-zero probability of producing the evidence field. Aggregating conditional PDFs resulted in a similar overall PDF with median M_w 7.3 and 95% CI of M_w 6.9- M_w 7.6, versus the actual M_w 6.7. Thus, the inversion framework significantly overpredicted the rupture magnitude, despite accurately predicting its location.

This discrepancy could have one or more causes. First, while epicentral grid points were converted to fault realizations using site-to-source distance correlations, these realizations may differ from the true source (e.g., with respect to fault orientation or depth). This will be further discussed later in the paper. Second, it can be seen in Fig. 10 that the fault ruptured beneath flat ground (i.e., on the edge of the San Joaquin Valley) and that this terrain extends a great distance east of the rupture location. As a result, very few landslides were observed at relatively short site-tosource distances, and none were observed east of the fault rupture. Analogous to the geolocation of earthquakes using seismic-wave arrivals, which relies on distributed seismic instruments, the proposed framework relies on distributed study sites (i.e., slopes with and without landslides) to "record" the ground motion. Thus, in events such as this, where the evidence field is constrained by topography and/or far from the source, it may be more difficult to detect the direction and rate of ground-motion attenuation, and therefore more difficult to constrain the source parameters. Third, the inversion framework relies on accurate predictions of ground-motions and landslides. Discrepancies between true and inverted seismic parameters are likely whenever these phenomena differ from expectations. An overpredicted magnitude could result, for example, if regional ground motions are greater than those predicted by the GMM, given the event magnitude (i.e., due to source, path, or site effects like topographic amplification). This could also result from landslides occurring more readily than expected, given the predicted ground motions. This is certainly plausible, given that the Nowicki et al. (2018) model does not consider local or regional variations in slope stratigraphy and material shear strength. Nonetheless, had the analysis been based on the Keefer (1984) magnitude-bound curve, a lower-bound estimate of M_w 5.4 would result, providing an equally poor constraint.

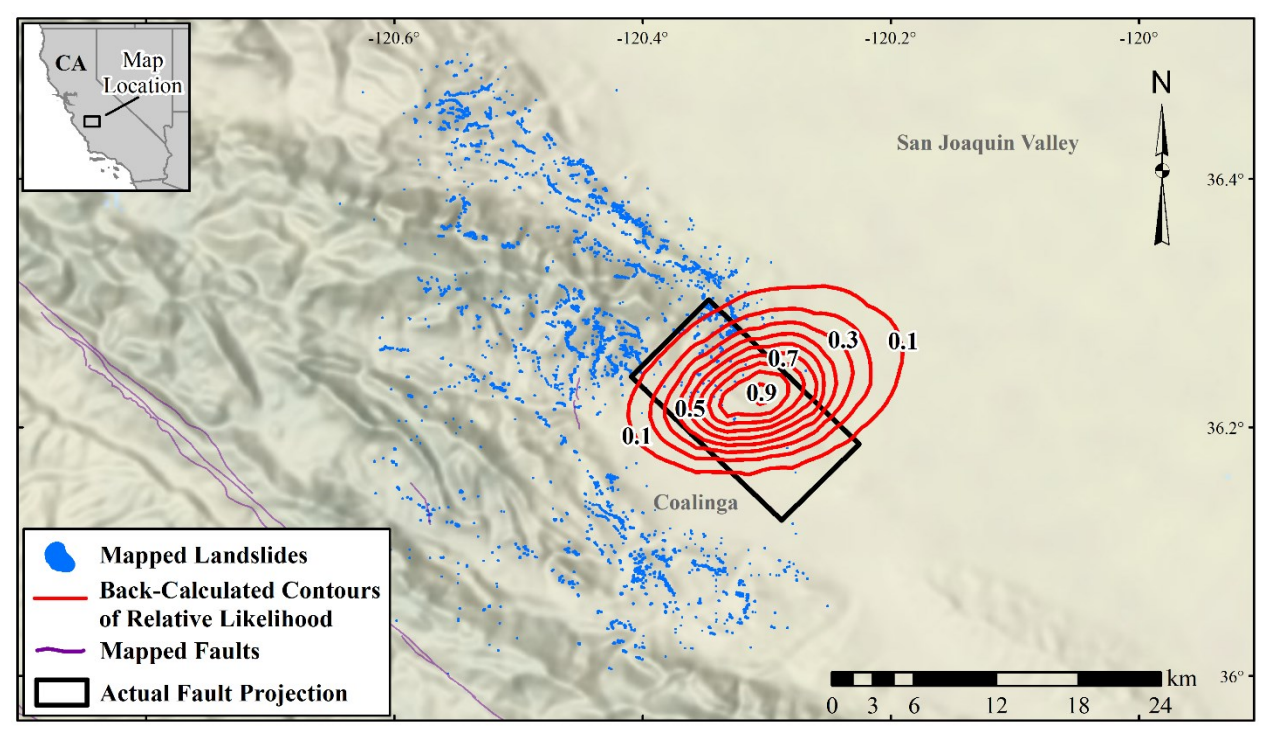


Fig. 10. Representative analysis of 100 study sites randomly selected from the 1983 M_w6.7 Coalinga earthquake inventory: contours showing the relative likelihood of source locations. Black rectangles = actual fault projection (Wentworth and Zoback 1990); faint purple lines = other mapped faults in the region (California Geological Survey 2014); blue polygons = complete inventory of mapped landslides.

4. Discussion and Conclusions

In regions where the modern earthquake catalog is poorly populated, analyses of paleolandslides may be used to infer information about the seismic hazard. However, existing analysis techniques: (i) require assumptions about the

causative earthquake's location, which can lead to inaccurate results; (ii) generally use only "positive" observations, leading to lower-bound estimates of M_w ; and (iii) have to-date been deterministic in nature, whereas paleolandslides involve multiple uncertainties. Accordingly, this paper proposed an approach by which seismic-source parameters are probabilistically constrained from regional landslide evidence, resulting in PDFs of rupture location and magnitude. Simulated paleoseismic studies were performed on four modern earthquakes in California, USA, wherein the analyses were blind to the actual source model (i.e., magnitude, location, geometry). While source parameters were accurately constrained in the 1971 San Fernando, 1989 Loma Prieta, and 1994 Northridge earthquakes, the analysis of the 1983 Coalinga earthquake highlighted possible limitations and lessons for use.

In these studies, provisional earthquake sources were modeled as epicenters and then converted to statistical fault realizations using empirical site-to-source distance correlations. For simplicity, and assuming the fault mechanism would be unknown in a paleoseismic study, an archetypical strike-slip fault was assumed, irrespective of the actual mechanism. However, because regional ground-motion patterns may be mechanism-dependent, the distribution of landslides can also vary, all else being equal (e.g., Tatard and Grasso 2013; Marc et al. 2017). The influence of fault mechanism might therefore be considered by repeating with other assumptions (i.e., normal, reverse) and coalescing the results via a logic tree. The branch weightings could be equal or informed by knowledge of the seismological setting (e.g., if one fault mechanism is believed to be more common). Alternatively, and while computationally demanding, the plausibility of 3-D source models could be directly evaluated with minimal modification. That is, the framework could quantify the likelihoods of faults with different strike, depth, mechanism, etc. producing an evidence field, so long as these faults result in different ground motions at landslide study sites. In this regard, because the framework relies on ground motions differing at different sites, it is generally best practice to compile spatially distributed study sites, given that multiple sites in proximity may provide little or no additional information. Given that the framework relies on predicting multiple phenomena in series, inaccuracies are likely whenever one or more of these phenomena differs from expectations. In the present study, the four application earthquakes were in California, USA, and were of relatively similar magnitude. Accordingly, these tests do not span the parameter space of geologic, seismologic, and climatic settings found on earth, nor do they include especially large- or small-magnitude events. However, because the framework is modular in nature, it can readily accommodate different ground-motion and landslide prediction models (e.g., region-specific models or models of differing complexity, depending on the availability of site-specific information). Above all, the framework remains conceptually valid for all earthquakes in all locations, so long as ground motions and landslides are predictable.

Given its modularity, the framework will also likely improve over time, since better component models are continuously proposed. In this regard, the Nowicki et al. (2018) landslide model was adopted herein for its ease of implementation to multiple earthquakes. In a paleolandslide study, wherein site- or region-specific profiling and material shear-strengths may be available, a more advanced model would potentially improve performance. Finally, the inversion framework, as demonstrated in this paper, did not simulate the field interpretation, dating, and inventorying prerequisite for inverse-analysis. As an example, and as in any paleolandslide study, the need exists to classify field observations as "positive" or "negative" (i.e., landslides did, or did not, occur). In practice, this presents a challenge, given the uncertain spatiotemporal potential for landslide evidence to be preserved in the geologic record. Inevitably, nearly all evidence from a given event is eventually erased. In such cases, the erroneous classification of a "positive" site as "negative" could result in the inverted, causative earthquake magnitude being less than actual. Similarly, a field of landslides interpreted to have resulted from one event could be augmented by additional spatially distributed earthquakes, or by weather events spaced closely in time. In such cases, the erroneous classification of a "negative" site as "positive" could result in the inverted, causative earthquake magnitude being greater than actual. As a result, the difficulty of accurate interpretation and analysis is likely to increase for increasingly older events. Additionally, the demonstrations presented herein used 100 randomly selected study sites, given the premise that a larger quantity would be unlikely in a paleoseismic study. It stands to reason, however, that: (i) analyses using a larger quantity of data are likely to be more accurate than those using a smaller quantity of data; and (ii) larger earthquakes impacting a larger geographic area are likely to require more data for accurate inversion, as compared to smaller earthquakes impacting a smaller area. To evaluate the finite-sample uncertainty of results (i.e., the uncertainty owed to incomplete data), the inversion can be repeated multiple times using bootstrap sampling, resulting in a distribution of PDFs. Inherently, this distribution would be wide when a small number of sites are studied (i.e., a different outcome could result from studying a different small number of sites) and narrow as the number of sites increases (i.e., the outcome would be relatively stable, regardless of which sites are studied). In this regard, uncertainties relating to field interpretation, evidence preservation, data selection, and temporal changes over long timescales were not present in the simulated studies of four modern earthquakes.

However, these applications did demonstrate how significant, quantifiable uncertainties can be accounted for via the total probability theorem, resulting in a probabilistic understanding of rupture location and magnitude, as inverted from landslide evidence. While paleolandslides have been studied and reported widely, less effort has arguably focused on advancing the methods for inverting seismic sources from field evidence. Towards that end, the approach proposed herein has the potential to provide new insights in regions of persistent seismic-hazard uncertainty.

5. Data Availability

All data analyzed herein is available in the public domain.

6. Supplemental Material

Appendix A, containing contour maps of most-likely M_w for each event, is available online.

7. Funding

The presented study is based on work supported by the National Science Foundation (NSF) under Grant No. CMMI-1751216, by the NSF Graduate Research Fellowship Program under Grant No. DGE-1762114, and by the University of Washington Royalty Research Fund (RRF). However, any opinions, findings, and conclusions or recommendations expressed in this paper are those of the authors and do not necessarily reflect the views of the NSF or RRF.

8. References

- Arino O, Ramos P, Jose J, Kalogirou V, Bontemps S, Defourny P, Van Bogaert E (2012) Global Land Cover Map for 2009 (GlobCover 2009). © European Space Agency (ESA) & Université catholique de Louvain (UCL), PANGAEA, https://doi.org/10.1594/PANGAEA.787668
- Atwater BF, Stuiver M, and Yamaguchi DK (1991) Radiocarbon test of earthquake magnitude at the Cascadia subduction zone. Nature 353: 156-158.
- Boulanger RW (2019) Nonlinear dynamic analyses of Austrian dam in the 1989 Loma Prieta earthquake. Journal of Geotechnical and Geoenvironmental Engineering 145(11): 05019011
- Bull WB, King J, Kong F, Moutoux T, Phillips WM (1994). Lichen dating of coseismic landslide hazards in Alpine mountains. Geomorphology 10:253–264. https://doi.org/10.1016/0169-555X(94)90020-5
- California Geological Survey (2014) Fault Activity Map of California. Scale not given. Accessed April 9, 2021, at: https://maps.conservation.ca.gov/cgs/fam/
- Carena S, Suppe J (2002). Three-dimensional imaging of active structures using earthquake aftershocks: the Northridge thrust, California. Journal of Structural Geology 24:887-904
- Chen XL, Zhou Q, Ran H, and Dong R (2012). Earthquake-triggered landslides in southwest China, Nat. Hazards Earth Syst. Sci., 12: 351-363, https://doi.org/10.5194/nhess-12-351-2012.
- Chiou BS-J and Youngs RR (2014) Update of the Chiou and Youngs NGA Model for the Average Horizontal Component of Peak Ground Motion and Response Spectra. Earthquake Spectra 30(3): 1117-1153.
- Clague J (2014) Paleolandslides. In: Davies T and Shroder F (Eds.) Landslide Hazards, Risks, and Disasters. Elsevier, pp 321-344
- Comerci V, Vittori E, Blumetti AM, Brustia E, Di Manna P, Gerrieri L, Lucarini M, and Serva, L. (2015) Environmental effects of the December 28, 1908, Southern Calabria-Messina (Southern Italy) earthquake. Nat Hazards 76: 1849-1891. https://doi.org/10.1007/s11069-014-1573-x.
- Crozier MJ (1992) Determination of paleoseismicity from landslides. In: Bell DH (ed) Landslides (Glissements de terrain), International Symposium, 6th, Christchurch, New Zealand, 1992, Proceedings: Rotterdam, A.A. Balkema, 2:1173-1180
- Danielson JJ, Gesch DB (2011) Global multi-resolution terrain elevation data 2010 (GMTED2010) U.S. Geological Survey Open-File Report 2011–1073, 26 p

- Delgado J, Garrido J, Lopez-Casado C, Martino S, Pelaez JA. (2011) On far field occurrence of seismically induced landslides. Engineering Geology 123:204-213. https://doi.org/10.1016/j.enggeo.2011.08.002
- Engelhart SE, Horton BP, Nelson AR, Hawkes AD, Witter RC, Wang K, Wang PL, and Vane CH (2013) Testing the use of microfossils to reconstruct great earthquakes at Cascadia. Geology 41 (10): 1067–1070.
- Geyin M, Baird AJ, Maurer BW (2020) Field assessment of liquefaction prediction models based on geotechnical versus geospatial data, with lessons for each. Earthquake Spectra 36(3):1386-1411.
- Goldfinger C, Nelson CH, Morey AE, Johnson JE, Patton JR, Karabanov E, Gutiérrez-Pastor J, Eriksson AT, Gràcia E, Dunhill G, Enkin RJ, Dallimore A, and Vallier T (2012) Turbidite event history methods and implications for Holocene paleoseismicity of the Cascadia subduction zone. U.S. Geological Survey Paper 1661–F, 170 pg.
- Harp EL, Jibson RW (1995) Inventory of landslides triggered by the 1994 Northridge, California earthquake. U.S. Geological Survey Open-File Report 95-213, 17 p., 2 pl. scale 1:50,000 and 1:100,000, available at: https://pubs.usgs.gov/of/1995/ofr-95-0213/
- Harp EL, Keefer DK (1990) Landslides triggered by the earthquake, in Rymer MJ, Ellsworth WL (eds.) The Coalinga, California, Earthquake of May 2, 1983, U.S. Geological Survey Professional Paper 1487, p. 335–347, 1 pl., scale 1:48,000, available at: https://pubs.usgs.gov/pp/1487/report.pdf
- Hartmann J, Moosdorf N (2012) The new global lithological map database GLiM: A representation of rock properties at the Earth surface. Geochemistry, Geophysics, Geosystems, 13, Q12004, https://doi.org/10.1029/2012GC004370
- Heath DC, Wald DJ, Worden CB, Thompson EM, Smoczyk GM (2020) A global hybrid VS 30 map with a topographic slope–based default and regional map insets. Earthquake Spectra 36 (3): 1570-1584.
- Hupp CR, Osterkamp WR and Thornton JL (1987) Dendrogeomorphic evidence and dating of recent debris flows on Mount Shasta, northern California. US Geol. Surv. Professional Paper 1396-B, 39 pp
- Jibson RW (1993) Predicting earthquake-induced landslide displacements using Newmark's sliding block analysis. Transportation research record 1411:9-17
- Jibson RW, Keefer DK (1993) Analysis of the seismic origin of landslides: Examples from the New Madrid seismic zone. Geol. Soc. Am. Bull. 105:421-436
- Jibson RW (1996) Use of landslides for paleoseismic analysis. Engineering Geology 43:291-323
- Johnson RH (1987) Dating of ancient, deep-seated landslides in temperate regions. In: MG Anderson, KS Richards (Eds.) Slope Stability. John Wiley and Sons, New York, pp 561-600
- Junquera-Torrado S, Moreiras SM, Rodriguez-Peces MJ, Sepulveda SA (2021) Linking earthquake-triggered paleolandslides to their seismic source and to the possible seismic event that originated them in a portion of the Argentine Precordillera (31°–33°S). Natural Hazards 106:43-78. https://doi.org/10.1007/s11069-020-04447-1
- Kaklamanos J, Baise LG, Boore DM (2011) Estimating unknown input parameters when implementing the NGA ground-motion prediction equations in engineering practice. Earthquake Spectra 27(4):1219-1235
- Katz O, Amit R, Yagoda-Biran G, Hatzor YH, Porat N, Medvedev B (2011) Quaternary earthquakes and landslides in the Sea of Galilee area, the Dead Sea Transform: paleoseismic analysis and implication to the current hazard. Isr. J. Earth Sci. 58:275–294. doi:10.1560/IJES.58.3-4.275
- Keefer, DK (1984) Landslides caused by earthquakes. Geol. Soc. Am. Bull. 95:406-421
- Keefer DK, Manson MW (1998) Regional distribution and characteristics of landslides generated by the earthquake, in Keefer DK (ed) The Loma Prieta, California, Earthquake of October 17, 1989—Landslides, U.S. Geological Survey Professional Paper, 1551-C, p. C7-C32, 4 pl., available at: https://pubs.usgs.gov/pp/pp1551/pp1551c/.
- Le Roux O, Schwartz S, Gamond JF, Jongmans D, Bourles D, Braucher R, Mahaney W, Carcaillet J, Leanni L (2009) CRE dating on the head scarp of a major landslide (Se'chilienne, French Alps), age constraints on Holocene kinematics. Earth and Planetary Science Letters 280:239–245. https://doi.org/10.1016/j.epsl.2009.01.034
- Mackey BH, Quigley MC (2014) Strong proximal earthquakes revealed by cosmogenic 3He dating of prehistoric rockfalls, Christchurch, New Zealand. Geology 42(11):975-978
- Martino S, Prestininzi A, and Romeo RW (2014) Earthquake-induced ground failures in Italy from a reviewed database. Nat. Hazards Earth Syst. Sci., 14: 799-814.
- Maurer BW, Green RA, Quigley MC, and Bastin S (2015) Development of magnitude-bound relations for paleoliquefaction analyses: New Zealand case study. Engineering Geology 197: 253-266.
- Meunier P, Uchida T, and Hovius N (2013) Landslide patterns reveal the sources of large earthquakes. Earth and Planetary Science Letters 36: 27-33.
- Morgenstern NU, Price VE (1965) The analysis of the stability of general slip surfaces. Geotechnique, 15(1):79-93 Morton DM (1971) Seismically triggered landslides in the area above the San Fernando Valley, in The San Fernando,
- California, Earthquake of February 9, 1971, U.S. Geological Survey Professional Paper 733, p. 99-109

- Nowicki Jessee MA, Hamburger MW, Allstadt K, Wald DJ, Robeson SM, Tanyas H, Hearne M, Thompson EM (2018) A Global Empirical Model for Near-Real-Time Assessment of Seismically Induced Landslides. Journal of Geophysical Research: Earth Surface 123(8):1835-1859. https://doi.org/10.1029/2017JF004494
- O'Donnell III RJ, Hawkes AD, Lane CS, Engelhard SE, Horton BP, Bobrowsky P, Sawai Y, Witter RC, Nelson AR, and Tanigawa K (2017) Assessing the utility of δ13C and bulk geochemistry in estuaries along the Cascadia subduction zone for coastal paleoseismology. Geological Society of America Abstracts with Programs 49(6): 58-2.
- Ojala AEK, Markovaara-Koivisto M, Middleton M, Ruskeeniemi T, Mattila J, Sutinen R (2018) Dating of paleolandslides in western Finnish Lapland. Earth Surf. Process. Landforms 43: 2449–2462.
- Panek T (2015) Recent progress in landslide dating: A global overview. Progress in Physical Geography: Earth and Environment 39(2):168-198. https://doi.org/10.1177/0309133314550671
- Papadopoulos GA, Plessa A (2000) Magnitude-distance relations for earthquake-induced landslides in Greece. Engineering Geology 58:377–386
- Peters R, Jaffe B, and Gelfenbaum G (2007) Distribution and sedimentary characteristics of tsunami deposits along the Cascadia margin of western North America. Sed Geo 200: 372-386.
- Petersen MD, Frankel AD, Harmsen SC, Mueller CS, Haller KM, Wheeler RL, Wesson RL, Zeng Y, Boyd OS, Perkins DM, Luco N, Field EH, Wills CJ, Rukstales KS (2008) Documentation for the 2008 update of the United States national seismic hazard maps. USGS Open-File Report 2008-1128, 61 p
- Petersen MD, Moschetti MP, Powers PM, Mueller CS, Haller KM, Frankel AD, Zeng Y, Rezaeian S, Harmsen SC, Boyd OS, Field N, Chen R, Rukstales KS, Luco N, Wheeler RL, Williams RA and Olsen AH (2014) Documentation for the 2014 update of the United States national seismic hazard maps. USGS Open-File Report 2014–1091, 243 p
- Rasanen RA, Marafi NA, and Maurer BW (2021) Compilation and forecasting of paleoliquefaction evidence for the strength of ground motions in the US Pacific Northwest. Engineering Geology 292: 106253.
- Rodríguez CE, Bommer JJ, Chandler RJ (1999) Earthquake-induced landslides 1980–1997. Soil Dynamics and Earthquake Engineering 18:325–346
- Scherbaum F, Schmedes J, Cotton F (2004) On the Conversion of Source-to-Site Distance Measures for Extended Earthquake Source Models. Bulletin of the Seismological Society of America 94(3):1053-1069
- Schmitt RG, Tanyas H, Nowicki Jessee MA, Zhu J, Biegel KM, Allstadt KE, Jibson RW, Thompson EM, van Westen CJ, Sato HP, Wald DJ, Godt JW, Gorum T, Xu C, Rathje EM, Knudsen KL (2017) An Open Repository of Earthquake-triggered Ground Failure Inventories. U.S. Geological Survey data release collection, accessed March 1, 2021, at https://doi.org/10.5066/F7H70DB4
- Stout ML (1977) Radiocarbon dating of landslides in southern California. California Division of Mines and Geology, California Geology, May 1977, pp 99-105
- Strasser M, Anselmetti FS, Fah D, Giardini D, Schnellmann M (2006) Magnitudes and source areas of large prehistoric northern Alpine earthquakes revealed by slope failures in lakes. Geology 34(12):1005-1008. https://doi.org/10.1130/G22784A.1
- Struble WT, Roering JJ, Black BA, Burns WJ, Calhoun N, Wetherell L (2020) Dendrochronological dating of landslides in western Oregon: Searching for signals of the Cascadia A.D. 1700 earthquake. GSA Bulletin 132(7-8): 1775–1791. https://doi.org/10.1130/B35269.1
- Sutinen R, Hyvonen E, Kukkonen, I (2014) LiDAR detection of paleolandslides in the vicinity of the Suasselka postglacial fault, Finnish Lapland. International Journal of Applied Earth Observation and Geoinformation 27:91–99. https://doi.org/10.1016/j.jag.2013.05.004
- Tanyaş, H, Allstadt KE, and van Westen CJ (2018) An updated method for estimating landslide-event magnitude. Earth Surf. Process. and forms 43: 1836-1847. https://doi.org/10.1002/esp.4359.
- Townsend KF, Gallen SF, Clark MK (2020) Quantifying near-surface rock strength on a regional scale from hillslope stability models: JGR Earth Surface 125(7). https://doi.org/10.1029/2020JF005665
- Updike RG, Brown WM, Johnson ML, Omdahl EM, Powers PS, Rhea S, Tarr AC (1996) USGS Response to an Urban Earthquake, Northridge '94. U.S. Geological Survey Open-File Report 96-263, 78 p
- USGS (2021) Ground Failure Scientific Background https://earthquake.usgs.gov/data/ground-failure/background.php. Accessed 01 March 2021
- Verdin KL (2017) Hydrologic Derivatives for Modeling and Applications (HDMA) database: U.S. Geological Survey data release, https://doi.org/10.5066/F7S180ZP
- Vidale J, Atkinson G, Green R, Hetland E, Grant-Ludwig L, Mazzotti S, Nishenko S and Sykes L (2011) Report of the independent expert panel on New Madrid Seismic Zone earthquake hazards as approved by NEPEC on April 16, 2011. U.S. Geological Survey, 26 p

- Wald DJ, Helmberger DV, Heaton TH (1991) Rupture Model of the 1989 Loma Prieta Earthquake from the Inversion of Strong-Motion and Broadband Teleseismic Data. Bulletin of the Seismological Society of America 81(5):1540-1572
- Wang B (2020) Geotechnical investigations of an earthquake that triggered disastrous landslides in eastern Canada about 1020 cal BP. Geoenvironmental Disasters (2020) 7:21. https://doi.org/10.1186/s40677-020-00157-9
- Watt JT, Brothers DA, Bennett SEK, Kluesner JW, Roland E, Conrad JE, Sliter RW, Dartnell P, Goldfinger C, Patton J, Michalak MJ, Sherrod BL, Gomberg J, and Wells RE (2017). "Toward a systematic characterization of Cascadia upper plate morphology, structure, and Quaternary deformation history: an integrated onshore-offshore approach." GSA Abstracts 49(6): 58.
- Wells DL, Coppersmith KJ (1994) New Empirical Relationships among Magnitude, Rupture Length, Rupture Width, Rupture Area, And Surface Displacement. Bulletin of the Seismological Society of America 84(4):974-1002
- Wentworth CM, Zoback MD (1990) Structure of the Coalinga Area and Thrust Origin of the Earthquake. In: Rymer MJ, Ellsworth WL (eds.) The Coalinga, California, Earthquake of May 2, 1983, U.S. Geological Survey Professional Paper 1487, p 417
- Yagoda-Biran G, Hatzor YH, Amit R, Katz O (2010) Constraining regional paleo peak ground acceleration from back analysis of prehistoric landslides: Example from Sea of Galilee, Dead Sea transform. Tectonophysics 490:81-92. https://doi.org/10.1016/j.tecto.2010.04.029